Effects of CO_2 on the Micron-Scale Pore-Fracture Structure and Connectivity in Coals from the Qinshui Basin

Shi-qi Liu[1(✉)], Shu-xun Sang[2], Tian Wang[2], Yi Du[2], and Hui-huang Fang[2]

[1] Jiangsu Key Laboratory of Coal-Based Greenhouse Gas Control and Utilization, Low Carbon Energy Institute, China University of Mining and Technology, Xuzhou, China
liushiqi@cumt.edu.cn

[2] Key Laboratory of Coalbed Methane Resources and Reservoir Formation Process, Ministry of Education, School of Mineral Resource and Geoscience, China University of Mining and Technology, Xuzhou, China

Abstract. The changes in the micron-scale pore and fracture structure in coal caused by CO_2 are critical to CO_2 injection and CH_4 output in coal seams. To investigate the effects of CO_2 on the characteristics and connectivity of micron-scale pores and fractures in coal, four coal samples from the Qinshui basin were selected. These samples were exposed to CO_2 and water for 240 h at 80 °C and 20 MPa using a CO_2 geochemical reactor. X-ray micro-CT (computed tomography), field emission scanning electron microscopy (FESEM), and energy dispersive spectroscopy (EDS) were used to identify the characteristics and connectivity of micron-scale pores and fractures in the coal samples before and after CO_2 treatment. Then, the influence of mineral dissolution on the micron-scale pores and fractures was discussed. After CO_2 treatment, the massive dissolution of carbonate minerals significantly increased the pore contents and volumes of the coal samples. For this reason, the grain size and volume of carbonate minerals determined the increase in pore number and volume after CO_2 treatment. The dissolution of calcite, dolomite, and other carbonate minerals in the coal matrix formed a large number of dissolution-created pores <10 μm in diameter, which affected the pore number in the coal after CO_2 treatment but contributed little to the coal connectivity at the micron-scale. Carbonate minerals filling micro-fractures were heavily dissolved by CO_2, which increased the aperture and connectivity of the micro-fractures. The dissolution of carbonate minerals in micro-fractures was the major contributor to the increase in the volume of pores >50 μm in diameter and the main reason for the increase in coal connectivity at the micron-scale.

Keywords: Connectivity · Pore diameter · Micro-fracture · Carbonate minerals · Qinshui basin

© The Author(s), under exclusive license to Springer Nature Singapore Pte Ltd. 2021
J. Lin (Ed.): IFEDC 2020, SSGG, pp. 504–521, 2021.
https://doi.org/10.1007/978-981-16-0761-5_50

1 Introduction

The adsorption of CO_2 is superior to that of CH_4 in coal seams [1, 2]. By injecting and storing CO_2 in coal seams, CH_4 can be displaced by CO_2 and expelled from the coal seam, thereby improving CH_4 recovery and reducing CO_2 emissions [2–4]. This technique is referred to as CO_2 geological storage-enhanced coalbed methane recovery (CO_2-ECBM). CO_2-ECBM has both environmental and energy benefits and has quickly become one of the hot spots in research on coalbed methane and emissions reduction [3, 4]. The United States, Canada, the Netherlands, Japan, and China have carried out pilot tests of CO_2-ECBM, and the results are satisfactory [4–7].

The mixing of CO_2 and water forms an acidic fluid containing H_2CO_3, which can dissolve calcite, dolomite, magnesite, and other minerals and promote the migration of Ca and Mg [8–13]. The CO_2-induced migration, dissolution and precipitation of inorganic minerals in coal change the coal structure, e.g., opening some closed and semi-closed pores in coal, changing the pore size distribution in coal, and increasing the coal porosity and permeability [14–19]. CO_2 can also dissolve minerals filling coal fractures, thus increasing the aperture and connectivity of coal fractures and changing the mechanical properties of the coal [14, 18, 20, 21]. Other scholars have suggested that the reaction between the CO_2-H_2O system and coal is a long-term process in which dissolved mineral components may migrate and precipitate in fractures that have not been filled by minerals or dissolved by CO_2, thereby reducing their connectivity [10, 15, 22, 23].

The characteristics and connectivity of pores and fractures in coal determine the storage, diffusion, and migration of CH_4 and CO_2 in coal [16, 24, 25]. It is generally believed that the micron-scale pores in coal are mainly secondary gas pores and dissolution-created pores, while the fractures are micro-fractures and some small-scale cleats [26–28]. These pores and fractures are the main seepage channels of CH_4 and CO_2 and connect the microscopic structure (e.g., adsorption pores and diffusion pores) and the macroscopic structure (e.g., macroscopic fractures) of coals [26–28]. Therefore, changes in the characteristics and connectivity of micron-scale pores and fractures in coal determine the injectivity and storage capacity of CO_2 and the production of CH_4, which are crucial factors in CO_2-ECBM. Research on the changes in coal structures caused by CO_2 reactions is mainly focused on the nano- to submicron-scale and the macro-scale. The changes in the characteristics and connectivity of pores and fractures at the micron-scale are still unclear. In this paper, using typical low-volatile bituminous coal and anthracite coal as examples, X-ray micro-CT (computed tomography), field emission scanning electron microscopy (FESEM), and energy disperse spectroscopy (EDS) were employed to describe the effects and mechanisms of CO_2 on the characteristics and connectivity of the micron-scale pores and fractures in coal. This study aims to provide a better understanding of the effectiveness of CO_2 injection and CH_4 production.

2 Samples and Methodology

2.1 Samples

Four groups of coal samples were collected in the Qinshui basin, China: low-volatile bituminous coal from the Xinyuan Mine, semi-anthracite coal from the Yuwu Mine and the Xinjing Mine, and anthracite coal from the Sihe Mine. These samples were named Coal #1 to Coal #4 (Table 1). The coal samples were systematically collected from working faces in the coal mines. The collection, retention, and preparation of the coal samples were conducted in line with the relevant standard GB/T 19222-2003 in China [29] and the international standard ISO 7404-2:1985. To prevent further oxidization, coal samples were wrapped in absorbent paper, hermetically sealed in plastic bags and stored at 5°C after sample collection. The key properties are shown in Table 1.

2.2 CO_2 Treatment

CO_2 treatments were performed to replicate a burial depth of 2000 m. The temperature and pressure at this burial depth (80 °C and 20 MPa, respectively) were calculated from the temperature and depth of the sub-surface constant temperature zone, the average geothermal gradient, and the average pressure gradient at the sampling location. The coal samples chosen for the CO_2 treatment consisted of small coal pillars for the X-ray CT scan and bulk coal for scanning electron microscopy (SEM) analysis. The details of the high-pressure reactor and experimental duration used in the CO_2 treatment can be found in our previous paper [13, 19]. After the CO_2 treatment, the coal samples were vacuum dried at 50 °C for 24 h for the X-ray CT scan and SEM analysis.

Table 1. Properties of the coals used.

Samples	Sampling location	*Ro*, max (%)	Proximate (wt %)				Ultimate (wt %)			
			M_{ad}	A_{ad}	V_{daf}	FC_{ad}	O_{daf}	C_{daf}	H_{daf}	N_{daf}
#1	Xinyuan Mine	1.81	0.81	5.35	15.26	80.20	9.30	80.32	4.43	1.14
#2	Yuwu Mine	2.19	1.10	11.98	13.44	76.19	2.44	91.73	4.12	2.44
#3	Xinjing Mine	2.64	1.66	10.02	10.10	80.89	3.05	91.52	3.96	1.06
#4	Sihe Mine	3.33	1.48	13.12	6.32	81.39	2.98	93.45	2.15	1.00

Note: *Ro*, max, the mean maximum reflectance values of vitrinite; wt %, weight percent; M_{ad}, moisture; A_{ad}, ash yield; V_{daf}, volatile matter; FC_{ad}, fixed carbon content; O_{daf}, oxygen content; C_{ad}, carbon content; H_{ad}, hydrogen content; N_{ad}, nitrogen content; "ad" means air-dried basis; "daf" means dry ash-free basis.

2.3 Pore-Fracture Network Modelling

X-ray CT Scan. X-ray CT scanning was performed with an Xradia 520 Versa X-ray CT scanner produced by the Carl Zeiss Foundation Group. Samples for X-ray CT scanning were small coal pillars approximately 2 mm in diameter and 2 mm in height. These were drilled from bulk coal samples using a mechanical sampler.

The scanning area of the X-ray CT scan was 1 mm in diameter and 1 mm in height. The total scan number was 1000, and the voxel resolution was 1.0 μm. After the X-ray CT scan, the small coal pillars were loaded into 800 mesh nylon bags that are resistant to high temperatures and corrosion for CO_2 treatment. After the CO_2 treatment, X-ray CT scans were again taken of the small coal pillars. To compare the X-ray CT results, the scanning range, total scan number, voxel resolution, and scanning position of the small coal pillars before and after CO_2 treatment were the same. To ensure the same scanning areas before and after CO_2 treatment, the central point of each small coal pillar was identified as the centre of the scanning area. Due to the manually set scanning area, slight errors may exist. However, the X-ray CT results show that these errors have a weak impact on the research and can be ignored.

Establishing the Pore-Fracture Network Model. Three-dimensional (3D) digital models of coal were established using Avizo 9, which is professional software for 3D digital cores based on X-ray CT images. The process of establishing the 3D digital model of the coal includes several steps, such as 3D imaging reconstruction, image denoising, image binarization, and model construction. Threshold selection is the key to identifying pores and fractures during the binarization process. In this paper, the X-ray CT images were first converted into 8-bit TIFF (Tag image file format) bitmaps, and then their greyscales were normalized to the range of 0–255. Thus, all bitmaps had 256 greyscales and the same grey range. Threshold segmentation of the X-ray CT images revealed that the grey ranges for pore fractures, organic matter, and minerals are 0–110, 110–180 and 180–255, respectively.

Based on the 3D digital model of coal, the characteristics of pores, fractures and minerals, including porosity, pore size distribution, pore volumes, mineral grain size distribution, and mineral volumes, were further extracted. The maximum inscribed ball method was used to extract pore size and mineral grain size, and the equivalent diameters (EqDiameters) of pores and minerals were obtained. Furthermore, the equivalent pore-fracture network models which are ball-and-stick models, and interconnected pore-fracture models, were established, and the coordination numbers of pores and fractures and throat lengths were extracted. Due to the large number of calculations and limited calculation capacity of the workstation, cubic ball-and-stick models and interconnected pore-fracture network models of coal samples that were 500 μm on each side were established.

According to the maximum inscribed ball method, fractures are filled with a number of balls and are cut into a number of pores. Therefore, the contents, volumes, and numbers of pores extracted from the 3D digital model contain the contents, volumes, and numbers of fractures. When establishing the ball-and-stick model, a series of balls filling the fractures are identified as throats. For this reason, fractures are generally considered throats in the ball-and-stick model.

2.4 Scanning Electron Microscopy Analysis

Pores, micro-fractures, and minerals in coal before and after CO_2 treatment were investigated using a Sigma 300 FESEM instrument produced by the Carl Zeiss Foundation Group, Germany, with a QUANTAX 200 EDS produced by Bruker

Company, USA, with amplification from 10^3 to 10^5. Samples used for FESEM were bulk coal. The coal samples were polished into small samples approximately 10–30 mm across and 4–5 mm high using a polishing and burnishing machine. Then, the small samples of coal were polished using a cross section polisher. After FESEM analysis, coal samples were first loaded into 800 mesh nylon bags for CO_2 treatment and then investigated again using FESEM to observe the changes in pores, fracture, and minerals after CO_2 treatment.

Coal is known as a non-conducting substance. Therefore, to achieve better experimental results, a thin gold coating is commonly applied to coal samples via sputtering. In this study, the gold coating can hamper the reactions between coal samples and CO_2. Therefore, instead of a gold coating, before CO_2 treatment, the subface and side faces of each coal sample were wrapped in conductive tape. After CO_2 treatment, to achieve better experimental results, a thin gold coating was applied to the coal samples via sputtering. The mineral grain size is small in coal, and minerals are difficult to locate. A photograph of the minerals was first taken using the backscattering mode with low amplification. With the help of the Advanced Mineral Identification and Characterization System (AMICS), the mineral compositions were initially identified, and the typical minerals were marked in the photographs. Then, using the secondary electron mode and by increasing the amplification step by step, details on the surface of typical minerals were observed. AMICS is the latest software package for automated identification and quantification of minerals and synthetic phases [10]. Combined with EDS, AMICS can be used to SEM image synthesis and automatically determine the compositions of minerals with grain sizes greater than 4 μm via an amplification of 200 [10].

3 Results and Discussion

3.1 Changes in Pore Structure

Pore Content. Before CO_2 treatment, the pore contents of coal samples are relatively low, ranging from 0.84–2.18% (Table 2). After CO_2 treatment, the pore contents (1.22–5.93%) of coal samples increase significantly, with an average increase of 82.61% (Table 2). The changes in pore volumes show the same trend as the pore contents (Table 2).

Table 2. Volumes and contents of pores and minerals in coal samples based on X-ray CT.

Samples	Pore content, %		Mineral content, %		Pore volume, μm^3		Mineral volume, μm^3	
	Before	After	Before	After	Before	After	Before	After
#1	2.18	3.33	5.43	3.33	1.62E+07	2.46E+07	4.01E+07	2.46E+07
#2	1.20	1.54	3.77	2.83	8.86E+06	1.14E+07	2.78E+07	2.09E+07
#3	1.95	5.93	8.18	3.73	1.48E+07	4.50E+07	6.22E+07	2.83E+07
#4	0.84	1.22	3.19	2.40	2.03E+07	2.98E+07	7.72E+07	5.86E+07

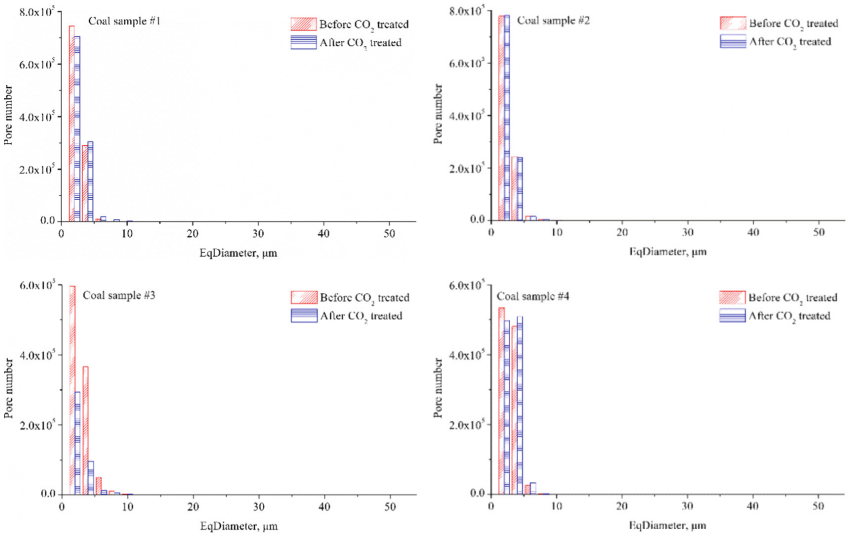

Fig. 1. Pore number distribution of coal samples based on X-ray CT.

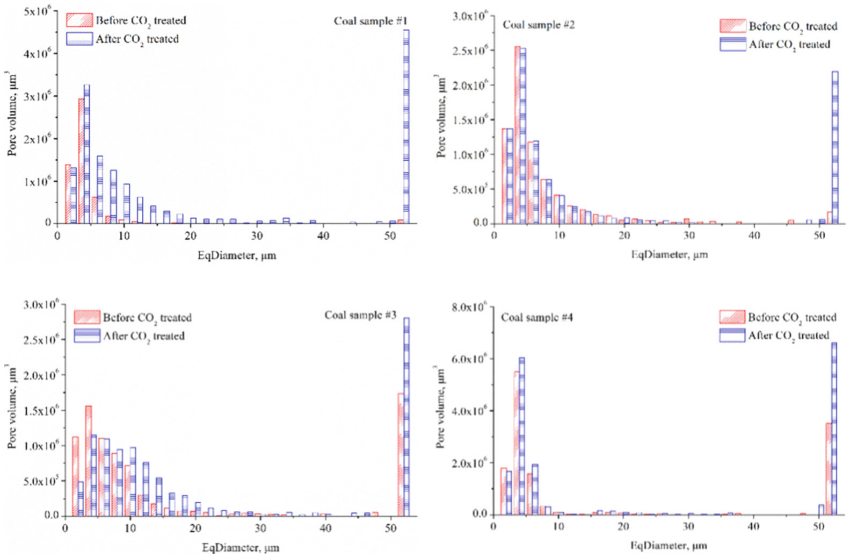

Fig. 2. Pore volume distributions of coal samples based on X-ray CT.

Pore Number. Before CO_2 treatment, the pores in the coal samples are primarily <5 μm in eqDiameter, and the pore number decreases rapidly with increasing pore eqDiameter (Fig. 1). The number of pores >10 μm in eqDiameter is small (Fig. 1). After CO_2 treatment, the number of pores <2 μm in Coal Sample #2 changes slightly, while the number in the other coal samples decreases (Fig. 1). The number of pores ranging from 2–10 μm in eqDiameter in Coal Sample #3 decreases, while the number

in the other coal samples increases slightly (Fig. 1). Moreover, the number of pores >10 μm in eqDiameter changes slightly (Fig. 1). In general, the changes in pore number are not significant, indicating that the changes in pore content and volume are not determined by changes in pore number.

Pore Volume. Before CO_2 treatment, the pore volumes of the coal samples are primarily associated with pores <10 μm in eqDiameter, with pores >10 μm in eqDiameter accounting for a small volume (Fig. 2). The volumes of pores <50 μm in eqDiameter are normally distributed, and the peak of pore volume is distributed from 3–4 μm (Fig. 2). With the increase and decrease in the pore eqDiameter, the pore volumes of the coal samples decrease rapidly (Fig. 2). Coal Sample #3 and Coal Sample #4 have larger volumes of pores >50 μm in eqDiameter, which may result from the presence of micro-fractures (Fig. 2). Combined with the pore number distribution, pores > 10 μm in eqDiameter contribute greatly to the pore volume. After CO_2 treatment, the pore volume distribution of the coal samples changes significantly, which is mainly caused by the significant increase in the volumes of pores >50 μm in eqDiameter (Fig. 2). In addition, the volumes of pores <50 μm in eqDiameter in Coal Sample #2 exhibit no marked changes, while the volumes of pores <4 μm in eqDiameter in Coal Sample #1, 3, and 4 decrease slightly (Fig. 2).

3.2 Changes in Connectivity

Interconnected Pore Models of Coal Samples. Before CO_2 treatment, there are a large number of pores and a certain number of micro-fractures in the 3D digital models of the coal samples (Fig. 3A). The 3D digital models and the ball-and-stick models show that micro-fractures are throats in the ball-and-stick models (Fig. 3B). Although some pores and micro-fractures are connected (Fig. 3B), the connectivity is weak, resulting in poor connectivity in the coal samples. Therefore, interconnected pore models of the coal samples cannot be extracted (Fig. 3C).

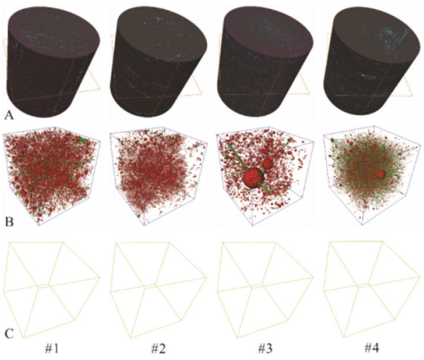

Fig. 3. 3D digital models, ball-and-stick models, and interconnected pore models of coal samples based on X-ray CT before CO_2 treatment. Notes: A, 3D digital models of coal; in the cubes, pores and micro-fractures are red, minerals are blue, and organic matter is grey; B, ball-and-stick models of pores and throats; in the ball-and-stick models, the pores are red, and the throats are green; and C, interconnected pore models.

After CO_2 treatment, some minerals filling pores and micro-fractures were dissolved, which increased the connectivity of pores and micro-fractures (Fig. 4A). The ball-and-stick models show that the number of interconnected pores and throats in the coal samples increase (Fig. 4B). However, the increase in connectivity of pores and micro-fractures caused by CO_2 does not obviously improve the connectivity of the coal samples on the macro-scale (Fig. 4C), and the connectivity of pores and micro-fractures is still limited to local areas in the coal samples and does not extend throughout the whole coal samples (Fig. 4C). After CO_2 treatment, the interconnected pore models of Coal Sample #1 and Coal Sample #2 were successfully extracted (Fig. 4C). By comparing the interconnected pore models and 3D digital models of Coal Samples #1 and #2, the connectivity of coal samples is improved by a micro-fracture (Fig. 4A, C), which means that the connectivity of coal samples on the micron-scale is mainly contributed by micro-fractures, while the contribution of pores is weak.

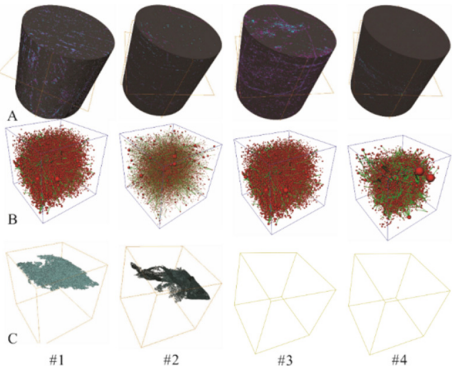

Fig. 4. 3D digital models, ball-and-stick models, and interconnected pore models of coal samples based on X-ray CT after CO_2 treatment.

Table 3. Numbers and contents of pores with different coordination numbers.

Samples	Pore number						Pore content, %			
	Before			After			Before		After	
	0	>0	Total	0	>0	Total	0	>0	0	>0
#1	1029934	16289	1046223	1005892	34226	1040118	98.44	1.56	96.71	3.29
#2	961181	81686	1042867	948262	94502	1042764	92.17	7.83	90.94	9.06
#3	1021998	5804	1027802	343714	69641	413355	99.44	0.56	83.15	16.85
#4	982578	60727	1043305	968959	73782	1042741	94.18	5.82	92.92	7.08

Notes: "0", pores with a coordination number of 0; ">0", pores with coordination numbers >0.

Coordination Numbers. The coal samples are dominated by isolated pores (pores with a coordination number of 0), and the number of pores with coordination numbers > 0 only account for 0.56–7.83% (Table 3). The coordination numbers of

interconnected pores (pores with coordination numbers >0) are low, primarily 1–2 (Fig. 5). The number of pores with a coordination number >2 decreases rapidly (Fig. 5), indicating that the connectivity of pores and fractures on the macro-scale is weak and that pores are only connected with 1–2 adjacent pores and throats.

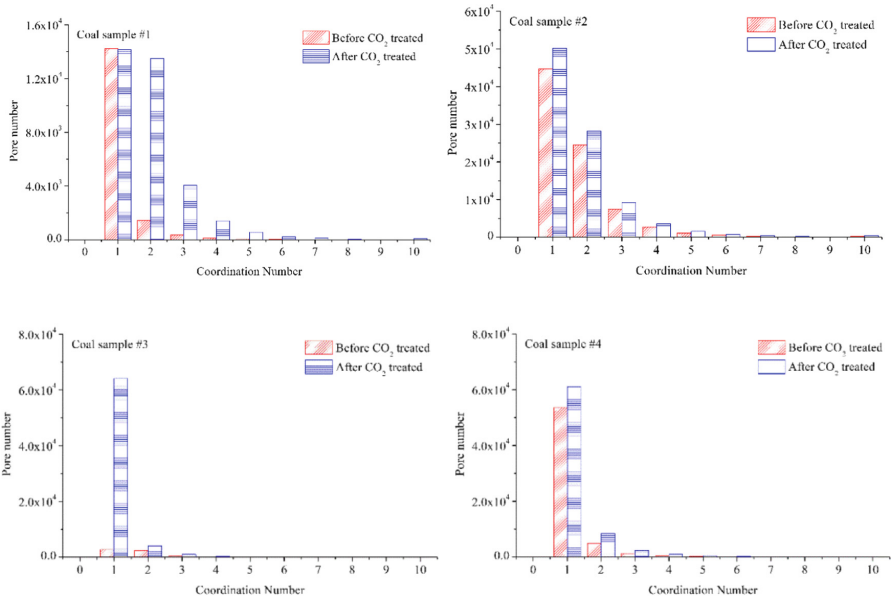

Fig. 5. Coordination numbers of coal samples based on X-ray CT.

After CO_2 treatment, the total number of pores in coal samples remained unchanged, except for Coal Sample #3 (Table 3). The number of pores with coordination numbers >0 increases, while the number of pores with a coordination number of 0 decreases correspondingly (Table 3), indicating that CO_2 improves the connectivity of pores in coal and has little influence on pore numbers. Although the total number of pores and the number of pores with a coordination number of 0 in Coal Sample #3 decrease, the number of pores with coordination numbers >0 increases significantly (Table 3). This is because a large number of pores in Coal Sample #3 become connected to form larger pores. The number of pores with coordination numbers >1 in coal samples all increases (Fig. 5), indicating that CO_2 improves the connectivity of pores and fractures in coal to a certain extent.

Throat Lengths. A throat is the connecting channel between pores and is representative of the connectivity of pores and fractures [30]. Before CO_2 treatment, throats <20 μm in length and >100 μm in length are most common (Fig. 6). Throats >100 μm in length are mainly composed of micro-fractures.

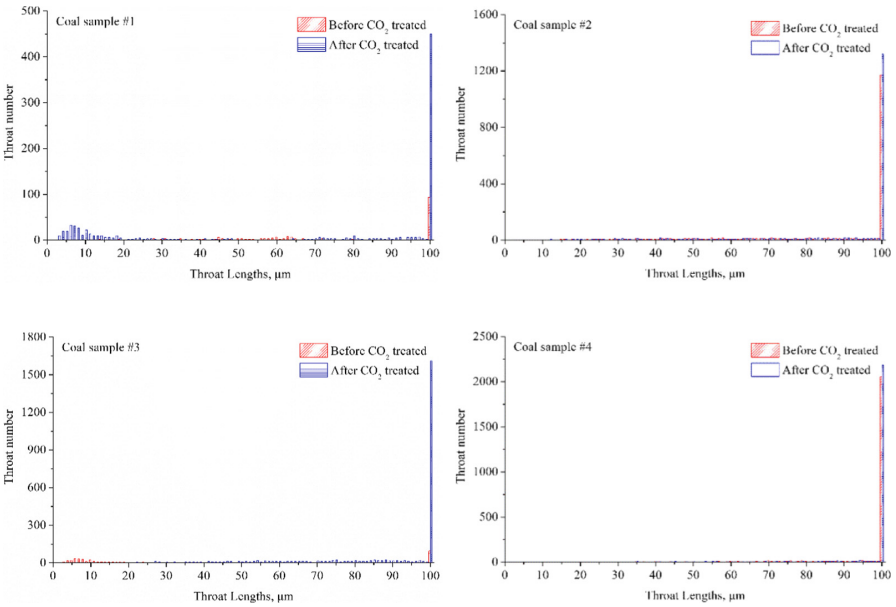

Fig. 6. Throat lengths of coal samples based on X-ray CT.

After CO_2 treatment, the number of throats >100 μm in length increases obviously (Fig. 6). The number of throats <100 μm in length in Coal Samples #2 and #4 changes weakly (Fig. 6). The number of throats <20 μm in length in Coal Sample #1 increases obviously, while the number in Coal Sample #3 decreases (Fig. 6). The number of throats 20–100 μm in length in Coal Sample #1 has no obvious change, while the number in Coal Sample #3 increases obviously (Fig. 6).

3.3 Changes in Minerals

Similar to the pore size distribution, the mineral grain size is mainly <5 μm, and as the grain size increases, the mineral number decreases rapidly (Fig. 7). Minerals with a grain size <50 μm are normally distributed, and the peaks of mineral volume are distributed at 3−6 μm (Fig. 8). With the increase and decrease in the grain size, the mineral volumes of coal samples decrease rapidly (Fig. 8). The volumes of minerals with grain sizes ranging from 10–50 μm are small, while those with grain sizes >50 μm are large (Fig. 8), indicating that there is a large amount of minerals with grain sizes >50 μm or a large amount of minerals filling the micro-fractures.

After CO_2 treatment, the mineral numbers show a significant decreasing tendency, while the number of minerals with grain sizes <6 μm in Coal Samples #1, #3, and #4 increases significantly, indicating that the minerals with grain sizes >6 μm are partially dissolved, resulting in a decrease in grain size (Fig. 7). After CO_2 treatment, the

volume of minerals with grain sizes >50 μm largely decreases (Fig. 8). Moreover, the 3D digital models of coal samples (Fig. 5A, Fig. 4A) show that minerals filling micro-fractures are largely dissolved by CO_2, which improves the connectivity of micro-fractures and increases the pore volume in the coal samples. Therefore, the dissolution of minerals with grain sizes >50 μm and filling micro-fractures is the main contributor to the decrease in mineral volume in the coal samples and the increase in the volume of pores >50 μm. Some minerals with grain sizes <50 μm are not completely dissolved, resulting in a significant decrease in the volume of minerals with grain sizes of 6–50 μm and a slight increase in the volume of minerals with grain sizes <6 μm in some coal samples (Fig. 8).

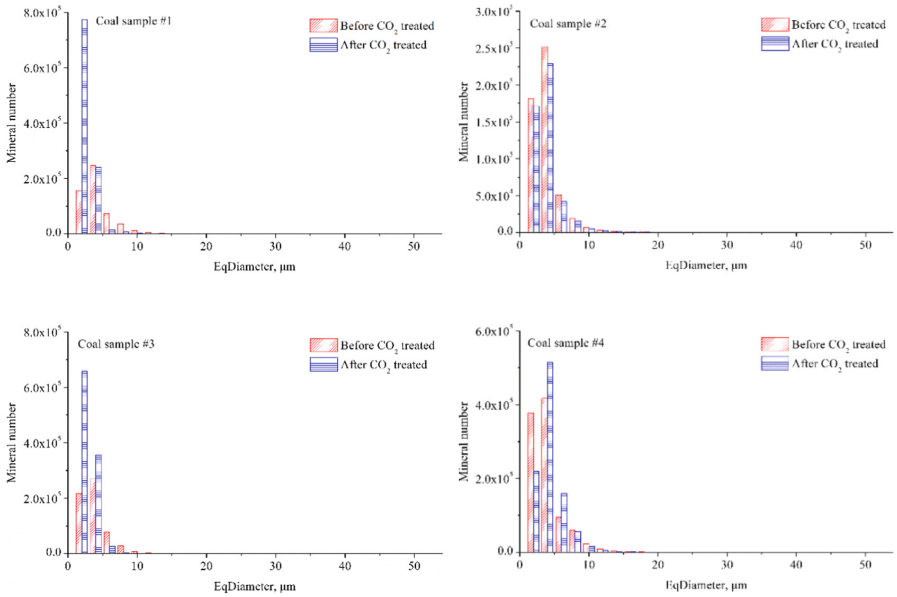

Fig. 7. Mineral number distributions of coal samples based on X-ray CT.

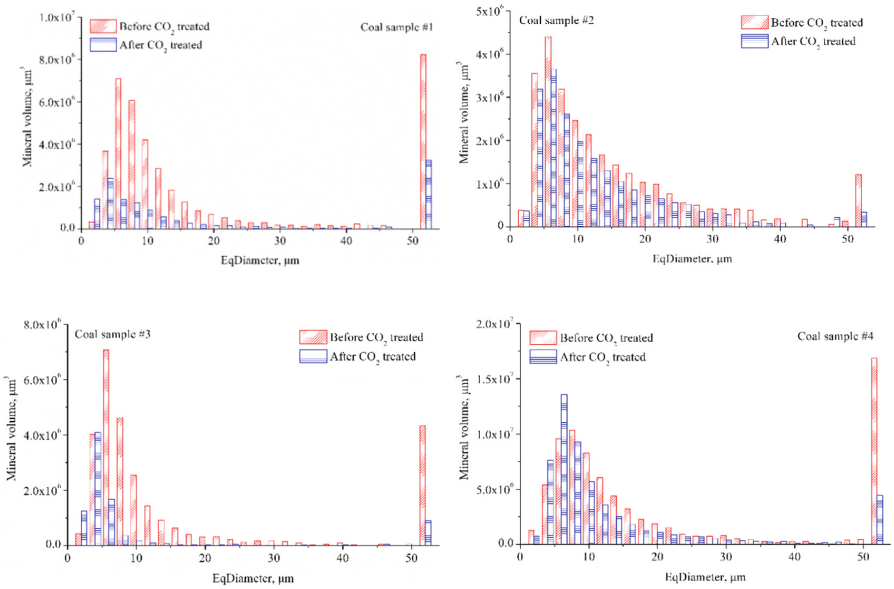

Fig. 8. Mineral volume distributions of coal samples based on X-ray CT.

3.4 Effects of Mineral Dissolution on the Pore Structure

The Relationship Between Pore Content and Mineral Dissolution. The mineral contents of the coal samples range from 3.19% to 8.18%, and these values decrease significantly (2.40–3.73%) after CO_2 treatment, with an average decrease of 35.69% (Table 2). After CO_2 treatment, significant positive correlations exists between the increase in pore content and the decrease in mineral content and between pore volume and mineral volume, with $R^2 = 0.8851$ and $R^2 = 0.9624$, respectively (Fig. 9). These relationships show that the change in pore content of the coal samples is closely related to the mineral dissolution caused by CO_2.

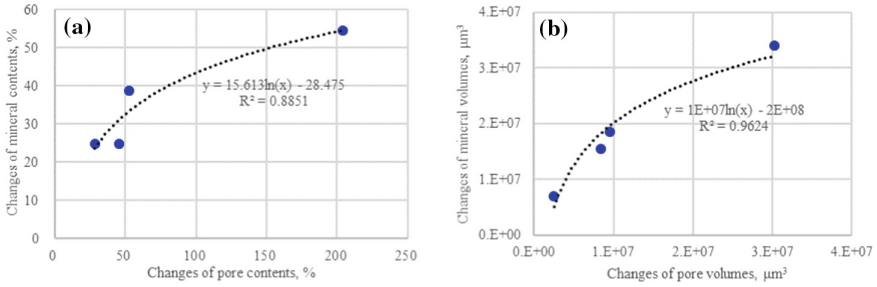

Fig. 9. Relationships between pores and minerals before and after CO_2 treatment.

Table 4. Area percentages of minerals in Coal Sample #2 before and after CO_2 treatment based on the EDS photos.

Mineral		Kaolinite	Calcite	Muscovite	Ankerite	Gibbsite	Dolomite	Organic-clay complexes	Other minerals
Area percentage, %	Before	46.01	15.98	13.52	1.60	2.48	0.15	5.28	14.98
	After	69.17	0.20	6.14	0.62	3.50	0.20	4.54	15.63

The Mechanism of the Effect of Mineral Dissolution on Pore Structure. The minerals with grain sizes >1 μm in the coal samples are mainly clay minerals and carbonate minerals. The clay minerals are mainly kaolinite (46.01%) and muscovite (13.52%), and the carbonate minerals include calcite (15.98%), ankerite (1.60%), and dolomite (0.15%). In addition, there is a certain amount of gibbsite (2.48%) and organic-clay complex (mainly organic-kaolinite complex) (5.28%) (Fig. 10, Table 4). The clay minerals are mainly distributed in the coal matrix, and the minerals filling the micro-fractures and pores are mainly carbonate minerals and gibbsite, as well as some organic-clay complexes (Fig. 10).

After CO_2 treatment, carbonate minerals are largely dissolved and disappear (Fig. 10 AA', BB'). Among them, calcite has the highest degree of dissolution and almost disappears (0.20%) (Table 4, Fig. 10 AA'), followed by ankerite filling micro-fractures (0.62%) (Table 4, Fig. 10 BB'). The dolomite in the coal matrix has a relatively low degree of dissolution (0.20%) (Table 4, Fig. 10 AA'), while the dolomite filling micro-fractures is largely dissolved (Fig. 10 CC'). Therefore, the dissolution of carbonate minerals is the main reason for the decrease in the mineral content in the coal. Kaolinite reacts weakly with CO_2. Therefore, kaolinite shows no significant change after CO_2 treatment (69.17%) (Table 4, Fig. 10 AA'). The gibbsite in the coal matrix is difficult to dissolve with CO_2 (Fig. 10 DD'), while the gibbsite filling the micro-fractures is partially dissolved (Fig. 10 CC'). Muscovite mainly exists in the coal matrix and can be partially dissolved by CO_2 (Fig. 10 AA'). The organic-clay complexes mainly fill micro-fractures and are partially dissolved by CO_2 (Fig. 10 BB').

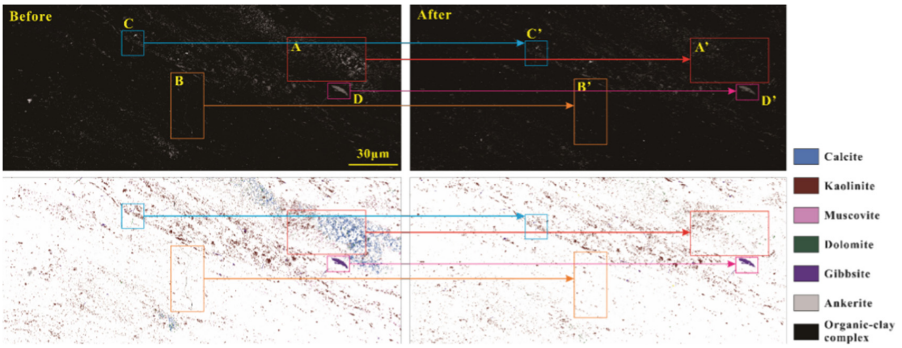

Fig. 10. The FESEM and EDS images of Coal Sample #2 before and after CO_2 treatment.

After CO_2 treatment, calcite, dolomite and other carbonate minerals in the coal matrix (including those filling pores) are dissolved or partially dissolved, forming a large number

of dissolution-created pores (Fig. 11a, c). The shape of these dissolution-created pores is irregular, and the pore diameter is generally <10 μm. Residual carbonate minerals can be found in these pores. These dissolution-created pores are the primary cause of the changes in the number and volume of pores <10 μm in diameter, and they control the changes in the pore number distribution in the coal samples (Fig. 11a, c). Some of the dissolution-created pores become connected with each other (Fig. 11a) and with micro-fractures (Fig. 11c); however, most of them are associated with local connectivity in a small part of coal samples, which are characterized by overall poor connectivity. Therefore, these pores make a weak contribution to the connectivity of the coal samples.

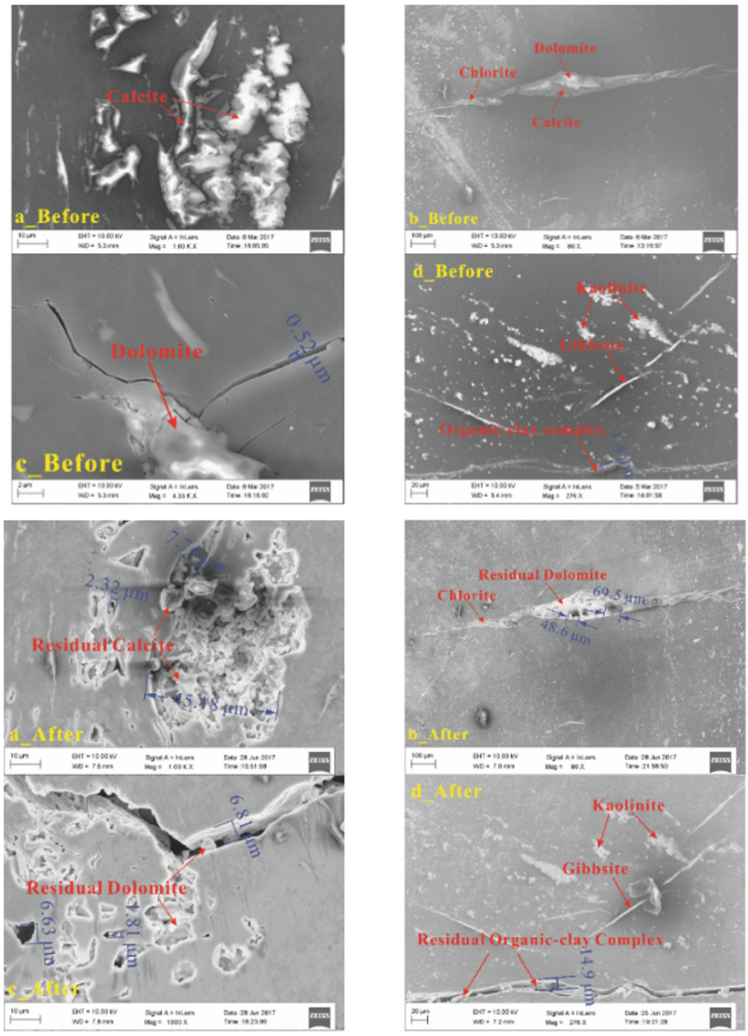

Fig. 11. Pores, micro-fractures, and minerals in coal samples before and after CO_2 treatment. Note: a and c are coal samples from the Xinjing Mine; c is a coal sample from the Sihe Mine; d is a coal sample from the Yuwu Mine.

After CO_2 treatment, the carbonate minerals, such as calcite and dolomite, with grain sizes >50 μm in the coal matrix (including those filling pores) are dissolved or partially dissolved, forming dissolution-created pores with diameters >50 μm (Fig. 11b). Residual carbonate minerals can also be found in the dissolution-created pores (Fig. 11b). These dissolution-created pores have a relatively large contribution to the number of pores >50 μm in diameter after CO_2 treatment, while they have a relatively small contribution to the pore volume. Similar to the dissolution-created pores <10 μm in diameter, the connectivity of the dissolution-created pores with diameters >50 μm is weak. A large number of carbonate minerals filling the micro-fractures are dissolved by CO_2, resulting in partial or complete opening of micro-fractures and significantly increasing the apertures of the micro-fractures (Fig. 11c). Although the number of micro-fractures is less than the number of dissolution-created pores >50 μm in diameter caused by CO_2 and has a much smaller contribution to the pore number, the volume of micro-fractures is much larger than that of dissolution-created pores >50 μm in diameter, and micro-fractures are the main contributor to the increase in the volume of pores >50 μm in diameter. This increase is also the reason that the pore volumes of the coal samples increase significantly after CO_2 treatment, while the pore numbers change only slightly. In addition, according to Sect. 3.2.3, the connectivity of coal samples on the micron-scale is mainly contributed by micro-fractures. Therefore, increasing the micro-fracture aperture significantly improves the connectivity of the coal samples and throat lengths. Moreover, some micro-fractures are filled with organic-clay complexes. After CO_2 treatment, a number of organic-clay complexes filling micro-fractures are removed, which also increases the apertures and connectivity of micro-fractures. In general, micro-fractures in coal samples are mainly filled with carbonate minerals (Fig. 10), and the removal of organic-clay complexes from micro-fractures has a relatively weak effect on micro-fractures. In addition, neither the clay minerals in the coal matrix nor the clay minerals filling the micro-fractures exhibit obvious changes after CO_2 treatment, and their influence on the pore-fracture structure and the coal connectivity is weak (Fig. 11d).

4 Conclusion

In this paper, taking low-volatile bituminous coals and anthracite coals collected from the Qinshui basin as examples, the changes in the pore-fracture structure and connectivity on the micron-scale after CO_2 treatments were discussed using X-ray micro-CT, FESEM, and EDS. The following conclusions can be drawn from this study.

(1) After CO_2 treatment, the pore contents and volumes of low-volatile bituminous coal and anthracite coal increase significantly, and the changes in pore numbers are small. The increase in pore volume is mainly caused by pores > 50 μm in diameter, while the change in pore number is related to pores <10 μm in diameter. The connectivity of low-volatile bituminous coal and anthracite coal on the micron-scale is mainly contributed by micro-fractures. After CO_2 treatment, the number of pores with coordination numbers >1 and the number of throats >100 μm in length increase significantly, confirming that CO_2 improves the

connectivity of pores and fractures; however, the improvement in pore-fracture connectivity is not enough to improve the connectivity of the coal on the micron-scale.

(2) After CO_2 treatment, the changes in pore numbers and volumes are mainly caused by the dissolution of carbonate minerals. Calcite, dolomite and other carbonate minerals in the coal matrix dissolve to form a large number of dissolution-created pores <10 μm in diameter. These dissolution-created pores are the main causes of the increase in the number and volume of pores <10 μm in diameter and determine the changes in pore numbers in coal samples. Carbonate minerals filling micro-fractures are greatly dissolved by CO_2, which increases the micro-fracture apertures and connectivity. These micro-fractures are the main contributor to the increase in the volume of pores >50 μm in diameter and improve the connectivity of coal on the micron-scale.

Acknowledgments. This study was supported by the National Key Research and Development Plan (No. 2018YFB0605601), the National Natural Science Foundation of China (No. 41972168), and the Foundation of Jiangsu Key Laboratory of Coal-based Greenhouse Gas Control and Utilization (No. 2019A001). We would like to thank engineers from the Shanxi CBM Branch of Huabei Oilfield Company and Lu'an Group and a number of research students from China University of Mining and Technology for their assistance in the coal sampling and some experiments.

References

1. Day, S., Duffy, G., Sakurovs, R., et al.: Effect of coal properties on CO_2 sorption capacity under supercritical conditions. Int. J. Greenhouse Gas Control **2**(3), 342–352 (2008)
2. White, C.M., Smith, D.H., Jones, K.L., et al.: Sequestration of carbon dioxide in coal with enhanced coalbed methane recovery - a review. Energy Fuels **19**(3), 659–724 (2005)
3. Hol, S., Gensterblum, Y., Massarotto, P.: Sorption and changes in bulk modulus of coal - experimental evidence and governing mechanisms for CBM and ECBM applications. Int. J. Coal Geol. **128–129**, 119–133 (2014)
4. Fujioka, M., Yamaguchi, S., Nako, M.: CO_2-ECBM field tests in the Ishikari Coal Basin of Japan. Int. J. Coal Geol. **82**(3), 287–298 (2010)
5. Faiz, M.M., Saghafi, A., Barclay, S.A., et al.: Evaluating geological sequestration of CO_2 in bituminous coals: the southern Sydney Basin, Australia as a natural analogue. Int. J. Greenhouse Gas Control **1**(2), 223–235 (2007)
6. Pan, Z., Ye, J., Zhou, F., et al.: CO_2 storage in coal to enhance coalbed methane recovery: a review of field experiments in China. **60**(5–6), 754-776 (2018)
7. Wong, S., Law, D., Deng, X.H., et al.: Enhanced coalbed methane and CO_2 storage in anthracitic coals - Micro-pilot test at South Qinshui, Shanxi, China. Int. J. Coal Geol. **1**(2), 215–222 (2007)
8. Bertier, P., Swennen, R., Laenen, B., et al.: Experimental identification of CO_2-water-rock interactions caused by sequestration of CO_2 in Westphalian and Buntsandstein sandstones of the Campine Basin (NE-Belgium). J. Geochem. Exploration **89**(1), 10–14 (2006)

9. Dawson, G.K.W., Golding, S.D., Biddle, D., et al.: Mobilisation of elements from coal due to batch reactor experiments with CO_2 and water at 40 °C and 9.5 MPa. Int. J. Coal Geol. **140**, 63–70 (2015)
10. Du, Y., Sang, S., Wang, W., et al.: Experimental study of the reactions of supercritical CO_2 and minerals in high-rank coal under formation conditions. Energy Fuels **32**(2), 1115–1125 (2018)
11. Hayashi, J., Takeuchi, K., Kusakabe, K., et al.: Removal of calcium from low rank coals by treatment with CO_2 dissolved in water. Fuel **70**(10), 1181–1186 (1991)
12. Kolak, J.J., Burruss, R.C.: The use of solvent extractions and solubility theory to discern hydrocarbon associations in coal, with application to the coal–supercritical CO_2 system. Org. Geochem. **73**, 56–69 (2014)
13. Liu, S.Q., Ma, J.S., Sang, S.X., et al.: The effects of supercritical CO_2 on mesopore and macropore structure in bituminous and anthracite coal. Fuel **223**, 32–43 (2018)
14. Anggara, F., Sasaki, K., Sugai, Y.: Mineral dissolution/precipitation during CO_2 injection into coal reservoir: a laboratory study. Energy Procedia **37**, 6722–6729 (2013)
15. Kutchko, B.G., Goodman, A.L., Rosenbaum, E., et al.: Characterization of coal before and after supercritical CO_2 exposure via feature relocation using field-emission scanning electron microscopy. Fuel **107**, 777–786 (2013)
16. Liu, C.J., Wang, G.X., Sang, S.X., et al.: Fractal analysis in pore structure of coal under conditions of CO_2 sequestration process. Fuel **139**, 125–132 (2015)
17. Liu, C.J., Wang, G.X., Sang, S.X., et al.: Changes in pore structure of anthracite coal associated with CO_2 sequestration process. Fuel **89**(10), 2665–2672 (2010)
18. Massarotto, P., Golding, S.D., Bae, J.S., et al.: Changes in reservoir properties from injection of supercritical CO_2 into coal seams - a laboratory study. Int. J. Coal Geol. **82**(3–4), 269–279 (2010)
19. Liu, S.Q., Sang, S.X., Ma, J.S., et al.: Effects of supercritical CO_2 on micropores in bituminous and anthracite coal. Fuel **242**, 96–108 (2019)
20. Perera, M.S.A., Ranjith, P.G., Choi, S.K., et al.: The effects of sub-critical and super-critical carbon dioxide adsorption-induced coal matrix swelling on the permeability of naturally fractured black coal. Energy **36**(11), 6442–6450 (2011)
21. Ranjith, P.G., Perera, M.S.A.: Effects of cleat performance on strength reduction of coal in CO2 sequestration. Energy **45**(1), 1069–1075 (2012)
22. Xu, Y.S., Liu, X.W., Zhang, P.H., et al.: Role of chlorine in ultrafine particulate matter formation during the combustion of a blend of high-Cl coal and low-Cl coal. Fuel **184**, 185–191 (2016)
23. Zerai, B., Saylor, B.Z., Matisoff, G.: Computer simulation of CO_2 trapped through mineral precipitation in the Rose Run Sandstone, Ohio. Appl. Geochem. **21**(2), 223–240 (2006)
24. Wang, A., Wei, Y., Yuan, Y., et al.: Coalbed methane reservoirs' pore-structure characterization of different macrolithotypes in the southern Junggar Basin of Northwest China. Mar. Pet. Geol. **86**, 675–688 (2017)
25. Zhou, H.W., Zhong, J.C., Ren, W.G., et al.: Characterization of pore-fracture networks and their evolution at various measurement scales in coal samples using X-ray μCT and a fractal method. Int. J. Coal Geol. **189**, 35–49 (2018)
26. Liu, S.Q., Sang, S.X., Liu, H.H., et al.: Growth characteristics and genetic types of pores and fractures in a high-rank coal reservoir of the southern Qinshui basin. Ore Geol. Rev. **64**, 140–151 (2015)
27. Liu, S.Q., Sang, S.X., Pan, Z.J., et al.: Study of characteristics and formation stages of macroscopic natural fractures in coal seam #3 for CBM development in the east Qinnan block, Southern Quishui Basin, China. J. Nat. Gas Sci. Eng. **34**, 1321–1332 (2016)

28. Liu, S.Q., Sang, S.X., Wang, G.X., et al.: FIB-SEM and X-ray CT characterization of interconnected pores in high-rank coal formed from regional metamorphism. J. Pet. Sci. Eng. **148**, 21–31 (2017)
29. Zhong, L.W., Chen, P.Y., Ren, D.Y.: China National Standards: Sampling of Coal Petrology (GB/T 19222-2003). Standards Press of China, Beijing (2003)
30. Song, W., Yao, J., Ma, J., et al.: Pore-scale numerical investigation into the impacts of the spatial and pore-size distributions of organic matter on shale gas flow and their implications on multiscale characterization. Fuel **216**, 707–721 (2018)